FLOW OF NANOWILLIAMSON FLUID WITH HEAT AND MASS TRANSFER THROUGH POROUS MEDIUM OVER AN EXPONENTIALLY PERMEABLE STRETCHING SHEET

Nabil T. M. Eldabe[1] , Kawther A. Kamel[2], Hameda M. Shawky[2] & Esmat A. Abd-Aziz [2]
[1]Department of Mathematics, Faculty of Education, Ain Shams University.
[2] Department of Mathematics, Faculty of Science, Al-Azhar University.
E-mail: esmat.abdel azeez@yahoo.com

ABSTRACT

This work examines the two-dimensional motion of non-Newtonain Williamson nano fluid with heat and mass transfer through porous medium over an exponentially stretching sheet. The system is stressed by an external uniform magnetic field and the thermal diffusion with chemical reaction and heat generation are considered. The system of partial differential equations which describe the momentum, energy and concentration equations of the fluid is transformed to an ordinary differential equations by using the suitable transformations. Then these equations have been solved numerically by using Runge-Kutta method based on shooting technique. The numerical formulas of the velocity, temperature and concentration are obtained. The effects of the physical parameters of the problem on these formulas are discussed and illustrated graphically. It is found that the physical parameters of the problem play an important rule to control the fluid flow.

1. Introduction

A nanofluid is a fluid in which nanometer-sized particles are suspended in a convectional heat transfer fluid to improve the heat transfer characteristics. Thus, nanofluids have many applications in industry such as coolants, iubricants, heatexchangers and micro-channel heat sinks One of the possible mechanisms for anomalous increase in the thermal conductivity of nanofluid is the Brownain motion of the nanoparticles inside the base fluids. A comprehensive survey of convective transport in nanofluids was made by Buongiorno [1]. The Buongiorno model [1] has been used by Khan and Pop [2] to study the boundary layer flow of a nanofluid past a stretching sheet. Kuznetsov and Nield [3] investigated the natural convective boundary-layer flow of a nanofluid past a vertical plate using Buongiorno model. Gorla and Chamkha [4] studied the natural convective boundary layer flow of nanofluid in a porous medium.

The effects of magneto hydrodynamics and thermal radiation on convective heat transfer play vital role in the phenomena of electrically conducting fluid past a heated surface and thermal processes involving high temperatures such as power generators, nuclear power plants. Swati [5] analysed these effects on boundary layer flow over an exponentially stretching sheet.

Chemical reaction effects on heat and mass transfer are of considerable importance in hydrometallurgical industries and chemical technology. Several investigators have examined the effect of chemical reaction on the flow, heat and mass transfer past a horizontal plate. Convective boundary-layer flow of MHD Nanofluid over a stretching surface with chemical reaction using the spectral relaxation method was studied by Haroun et al. [6]. Recently, Kiran Kumar et al. [7,8] analyzed the study of heat and mass transfer enhancement in free convection flow with chemical reaction and thermo-diffusion in nanofluids through porous medium in a rotating frame.

In non-Newtonian fluids, the most commonly encountered fluids are pseudoplastic fluids. The study of the boundary layer flow of pseudoplastic fluids is of great interest due to its wide range of application in industry such as extrusion of polymer sheets, emulsion coated sheets like photographic films, solutions and melts of high molecular weight polymers, etc. the Navier Stokes equations along are insufficient to explain the rheological properties of fluids. Therefore, rheological models have been proposed to overcome this deficiency. To explain the behavior of pseudoplastic fluids many models have been proposed like the power law model, Carreaus model, Cross model and Ellis model, but little attention has been paid to the Williamson fluid model. Williamson [9]

discussed the flow of pseudoplastic materials and proposed a model equation to describe the flow of pseudoplastic fluids and experimentally verified the results. Lyubimov and Perminov [10] discussed the flow of a thin layer of a Williamson fluid over an inclined surface in the presence of a gravitational field. Dapra and Scarpi [11] developed the perturbation solution for a Williamson fluid injected into a rock fracture. Peristaltic flow of a Williamson fluid has been discussed by Nadeem *et al.* [12]. Vasudev *et al.* [13] studied the peristaltic pumping of a Williamson fluid through a porous medium considering heat transfer. Cramer *et al.* [14] showed that this model fits the experimental data of polymer solution and particle suspensions better than other models. For pseudoplastic fluids the power law model predicts that the apparent/effective viscosity should decrease indefinitely with increasing shear rate, which means infinite viscosity at rest and zero viscosity as the shear rate approaches infinity. A real fluid has both minimum and maximum effective viscosities depending upon the molecular structure of the fluid. In the Williamson fluid model, both the minimum (μ_0) and maximum viscosities (μ_∞) are considered. So, for pseudoplastic fluids (for which the apparent viscosity does not go to zero at infinity), it will give better results.

In this paper, our aim is study the two-dimensional Williamson nanofluid flows over permeable exponentially stretching sheet in a porous medium with a transverse magnetic field, taking into account the effects of viscous dissipation, chemical reaction, heat generation, ohmic effect in the momentum and energy equations respectively. The governing equations are transformed into nonlinear ordinary differential equations by using similarity transformation and then solved numerically using Runge-Kutta based shooting technique. The effects of various governing parameters on the fluid velocity, temperature, nanoparticle volume friction, Nusselt number and nanoparticale volume friction gradient are shown in figures and analyzed in detail.

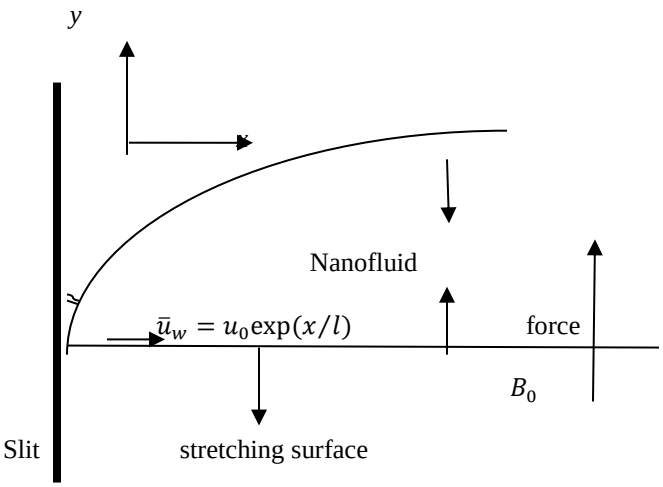

Figure 1 Sketch of the physical model.

2. Mathematical Formulation

Consider a steady two-dimensional flow of an electrically conducting incompressible nano Williamson fluid over a stretching surface in the region $y > 0$, we used a (x, y) coordinate system. Keeping the origin fixed, two equal and opposite forces are applied along the x-axis which results in stretching of the surface and a uniform magnetic field of strength B_0 is imposed along the y-axis. The plate is stretched along x-axis with a velocity $U_w = U_0 \exp(x/l)$, see (Fig. 1). the chemical reaction and heat generation are taking place in the flow. The flow is generated due to the linear stretching. In the absence of a body force, the governing equations can be written as:

$$div\, V = 0, \tag{1}$$

$$\rho \frac{dV}{dt} = div\, S + \rho b - \frac{\mu}{k} V + \bar{J} \wedge \bar{B}, \tag{2}$$

$$(\rho c)_f\left(\frac{\partial T}{\partial t}+V.\nabla T\right)=\nabla.k_T\nabla T+\rho_P c_P\times\left(D_B\nabla C.\nabla T+D_T\frac{\nabla T.\nabla T}{T_\infty}\right)+\varphi+\frac{1}{\sigma}(\bar{J}.\bar{J})+Q_0(T-T_\infty)\ (3)$$

$$\frac{\partial C}{\partial t}+V.\nabla C=\nabla.\left(D_B\nabla C+D_T\frac{\nabla T}{T_\infty}\right)-k_1(C-C_\infty)\qquad(4)$$

where ρ is nanofluid density, V is the velocity vector, S is the Cauchy stress tensor, b represents the specific body force vector and d/dt represents the material time derivative, ρ_c and $\rho_p c_p$ are heat capacities of nanofluid and nanoparticles, respectively, T and T_∞ are temperature, k is nanofluid thermal conductivity, D_B is Brownian diffusion coefficient, C is nanoparticle volumetric fraction, D_T is thermophoretic diffusion coefficient, $\varphi=\tau_{IJ}\frac{\partial u_i}{\partial x_j}$ is the dissipation function (viscous dissipation), T_∞ and C_∞ are the ambient fluid temperature and concentration respectively, Q_0 and k_1 are the rate of heat generation and chemical reaction respectively.

The constitutive equations of the Williamson fluid model are given as:

$$S=-pI+\tau,\qquad(5)$$

$$\tau=\left[\mu_\infty+\frac{(\mu_0-\mu_\infty)}{1-\Gamma\dot{\gamma}}\right]A_1,\qquad(6)$$

in which p is the pressure, I is the identity vector, $\boldsymbol{\tau}$ is the stress tensor, μ_0 and μ_∞ are the limiting viscosities at zero and at infinite shear rate, $\Gamma>0$ is the time constant, A_1 is the first Rivlin- Erickson tensor and $\dot{\gamma}$ is defined as follows

$$A_{(1)ij}=V_{i,j}+V_{j,i}\qquad(7)$$

$$\dot{\gamma}=\sqrt{\frac{1}{2}\Pi},\qquad(8)$$

$\Pi=$ trace $(A_1{}^2)$,

$$\dot{\gamma}=\left[\left(\frac{\partial u}{\partial x}\right)^2+\frac{1}{2}\left(\frac{\partial u}{\partial y}+\frac{\partial v}{\partial x}\right)^2+\left(\frac{\partial v}{\partial y}\right)^2\right]^{1/2},\qquad(9)$$

where Π is the second invariant strain tensor. Here we have only considered the case for which $\mu_\infty=0$ and $\Gamma\dot{\gamma}<1$. Thus, the extra stress tensor takes the form:

$$\tau=\left[\frac{\mu_0}{1-\Gamma\dot{\gamma}}\right]A_1,\qquad(10)$$

by using binomial expansion, we get:

$$\tau=\mu_0[1+\Gamma\dot{\gamma}]A_1,\qquad(11)$$

The components of the extra stress tensor are:

$$\tau_{xx}=2\mu_0[1+\Gamma\dot{\gamma}]\frac{\partial u}{\partial x},$$

$$\tau_{xy} = \tau_{yx} = \mu_0[1 + \Gamma\dot{\gamma}]\left(\frac{\partial u}{\partial x} + \frac{\partial v}{\partial y}\right),$$

$$\tau_{yy} = 2\mu_0[1 + \Gamma\dot{\gamma}]\frac{\partial v}{\partial y}\ , \qquad (12)$$

$$\tau_{xz} = \tau_{yz} = \tau_{zx} = \tau_{zy} = \tau_{zz} = 0,$$

The interaction of magnetic field and velocity will give rise to the Lorentz force $J \times B$**,** where

$J = \sigma(E + V \times B)$

Then equations (1-12) in two-dimensional form can be written as:

$$\frac{\partial u}{\partial x} + \frac{\partial v}{\partial y} = 0, \qquad (13)$$

where *u(x,y)* and *v(x,y)* are the velocity components along the flow direction and the normal to the flow direction, respectively:

$$\rho_f\left(u\frac{\partial u}{\partial x} + v\frac{\partial u}{\partial y}\right) = -\frac{\partial p}{\partial x} + \frac{\partial \tau_{xx}}{\partial x} + \frac{\partial \tau_{xy}}{\partial y} - \sigma B_0^2 - \frac{\mu}{k}u, \qquad (14)$$

$$\rho_f\left(u\frac{\partial v}{\partial x} + v\frac{\partial v}{\partial y}\right) = -\frac{\partial p}{\partial y} + \frac{\partial \tau_{yx}}{\partial x} + \frac{\partial \tau_{yy}}{\partial y} - \frac{\mu}{k}v, \qquad (15)$$

$$(\rho c)_f\left(u\frac{\partial T}{\partial x} + v\frac{\partial T}{\partial y}\right) = k_T\frac{\partial^2 T}{\partial y^2} + \rho_P C_P\left(D_B\frac{\partial C}{\partial y}\frac{\partial T}{\partial y} + \frac{D_T}{T_\infty}\left(\frac{\partial T}{\partial y}\right)^2\right) + \tau_{xx}\frac{\partial u}{\partial x} + \tau_{yy}\frac{\partial v}{\partial y} + \tau_{xy}\left(\frac{\partial u}{\partial x} + \frac{\partial v}{\partial y}\right) + (\sigma B_0^2)u^2 + Q_0(T - T_\infty), \qquad (16)$$

$$u\frac{\partial C}{\partial x} + v\frac{\partial C}{\partial y} = D_B\frac{\partial^2 C}{\partial y^2} + \frac{D_T\partial^2 T}{T_\infty\partial y^2} - k_1(C - C_\infty), \qquad (17)$$

where $\tau_{xx}, \tau_{xy}, \tau_{yy}$ are the components of the extra stress tensor Eq. (12).

$$\frac{\tau_{xx}}{\rho_f} = \frac{2\mu_0}{\rho_f}\left[\frac{\partial u}{\partial x} + \Gamma\frac{\partial u}{\partial x}\left\{\left(\frac{\partial u}{\partial x}\right)^2 + \frac{1}{2}\left(\frac{\partial u}{\partial y} + \frac{\partial v}{\partial x}\right)^2 + \left(\frac{\partial v}{\partial y}\right)^2\right\}^{1/2}\right], \qquad (18)$$

$$\frac{\tau_{xy}}{\rho_f} = \frac{\mu_0}{\rho_f}\left[1 + \Gamma\left\{\left(\frac{\partial u}{\partial x}\right)^2 + \frac{1}{2}\left(\frac{\partial u}{\partial y} + \frac{\partial v}{\partial x}\right)^2 + \left(\frac{\partial v}{\partial y}\right)^2\right\}^{1/2}\right], \qquad (19)$$

$$\frac{\tau_{yy}}{\rho_f} = \frac{2\mu_0}{\rho_f}\left[\frac{\partial v}{\partial y} + \Gamma\frac{\partial v}{\partial y}\left\{\left(\frac{\partial u}{\partial x}\right)^2 + \frac{1}{2}\left(\frac{\partial u}{\partial y} + \frac{\partial v}{\partial x}\right)^2 + \left(\frac{\partial v}{\partial y}\right)^2\right\}^{1/2}\right]. \qquad (20)$$

equations (13-17) after using the expressions of τ_{xx}, τ_{xy} and τ_{yy} can be written as:

$$\frac{\partial u}{\partial x} + \frac{\partial v}{\partial y} = 0, \qquad (21)$$

$$u\frac{\partial u}{\partial x} + v\frac{\partial u}{\partial y} = -\frac{1}{\rho_f}\frac{\partial p}{\partial x} + \nu\frac{\partial^2 u}{\partial y^2} + \sqrt{2}\nu\Gamma\frac{\partial u}{\partial y}\frac{\partial^2 u}{\partial y^2} - \frac{\sigma}{\rho_f}B_0^2 - \frac{\mu}{\rho_f k}u, \qquad (22)$$

$$\frac{\partial p}{\partial y} = 0, \qquad (23)$$

$$u\frac{\partial T}{\partial x} + v\frac{\partial T}{\partial y} = \alpha\frac{\partial^2 T}{\partial y^2} + \frac{\rho_P C_P}{(\rho_C)_f}\left(D_B\frac{\partial C}{\partial y}\frac{\partial T}{\partial y} + \frac{D_T}{T_\infty}\left(\frac{\partial T}{\partial y}\right)^2\right) + \frac{\mu_f}{(\rho c)_f}\left(\frac{\partial u}{\partial y}\right)^2 + \frac{\mu_f\,\Gamma}{\sqrt{2}(\rho c)_f}\left(\frac{\partial u}{\partial y}\right)^3 + \left(\frac{\sigma B_0^2}{(\rho c)_f}\right)u^2 + \frac{Q_0}{(\rho c)_f}(T - T_\infty), \qquad (24)$$

$$u\frac{\partial C}{\partial x}+v\frac{\partial C}{\partial y}= D_B\frac{\partial^2 C}{\partial y^2}+\frac{D_T\partial^2 T}{T_\infty\partial y^2}-k_1(C-C_\infty), \quad (25)$$

where ν is the kinematic viscosity, $\alpha=\frac{k_T}{(\rho c)_f}$ is the thermal diffusivity of the base fluid and σ is the Steffan-Boltzman constant.

The corresponding boundary conditions are given by

$$u=U_w(x)=U_0 exp\left(\frac{x}{l}\right),\quad v=-\beta(x)\ ,\ \ T=T_w\ ,\ C=C_w\ ,\text{ at}\quad y=0$$

$$u=0\ ,\qquad T=T_\infty,\qquad C=C_\infty,\qquad \text{as } y\to\infty. \quad (26)$$

in which U_0 is the reference velocity, $\beta(x)$ is the suction and injection velocity when $\beta(x)>0$ and $\beta(x)<0$ respectively. The fluid velocity, temperature and nanoparticle concentration near surface are assumed to be U_w, T_w and C_w, respectively.

Introduce the following transformations in Eqs. (22)-(25):

$$\left.\begin{aligned} &u=U_0 exp\left(\frac{x}{l}\right)f'(\eta),\\ &v=-\sqrt{\frac{\nu U_0}{2l}}exp\left(\frac{x}{2l}\right)\{f(\eta)+\eta f'(\eta)\},\\ &\eta=y\sqrt{\frac{U_0}{2\nu l}}exp\left(\frac{x}{2l}\right),\qquad \theta=\frac{T-T_\infty}{T_w-T_\infty},\qquad \emptyset=\frac{C-C_\infty}{C_w-C_\infty}, \end{aligned}\right\} \quad (27)$$

in above expression, η the dimensionless variable and *f'*, θ and $\emptyset$ are dimensionless velocity, temperature and concentration, respectively. Thus by neglecting pressure gradient in the *y*-direction, the equation of linear momentum, energy and concentration in dimensionless form became:

$$f'''-2f'^2+ff''+\lambda f''f'''-2(M+K)f'=0, \quad (28)$$

$$\theta''+P_r f\theta'+\frac{N_c}{Le}\phi'\theta'+\frac{N_c}{Le\times N_{bt}}\theta'^2+B_r f''^2+\frac{1}{\sqrt{2}}B_r\lambda f''^3+2MB_r f'^2+2RePrQ\theta=0$$

(29)

$$\emptyset''+Scf\emptyset'+\frac{1}{N_{bt}}\theta''-2ReS_C K_r\phi=0, \quad (30)$$

prime denotes derivative w.r.t η.

The corresponding boundary conditions are

$$\left.\begin{aligned} &f=v_w,\qquad f'=1,\qquad \theta=1,\qquad \phi=1,\qquad \text{at } \eta=0\\ &f'\to 0,\qquad \theta\to 0,\qquad \emptyset\to 0,\qquad \text{as}\quad \eta\to\infty \end{aligned}\right\} \quad (31)$$

In above transformed equations the following non-dimensional parameters are introduced:

$\lambda=\Gamma\sqrt{\frac{U_0^3 exp(3x/l)}{\nu\, l}}$ (Non Newtonain Williamson parameter),

$P_r=\frac{\nu}{\alpha}$ (Prandtl number = momentum diffusivity/ nanofluid thermal diffusivity),

$Le = \frac{\alpha}{D_B}$ (Lewis number = nanofluid thermal diffusivity/Brownian diffusivity),

$S_c = \frac{\nu}{D_B}$ (Schmidt number = momentum diffusivity/ Brownian diffusivity),

$N_c = \frac{\rho_P C_P}{\rho_C}(C_w - C_\infty)$(Heat capacities ratio = nano particles heat capacity/ nanofluid heat capacity),

$N_{bt} = \frac{D_B T_\infty (C_W - C_\infty)}{D_T (T_W - T_\infty)}$ (Diffusivity ratio = Brownian diffusivity/ thermophoretic diffusivity),

$B_r = P_r E_c$ (Brinkmen number)viscous heating,

$Re = \frac{U_w l}{\nu}$ (Local Renolds number),

$Q = \frac{Q_0 \nu}{(\rho c)_f U_w^2}$ (Heat generation parameter),

$K_r = \frac{K_1 \nu}{U_w^2}$ (Chemical reaction parameter),

$M = \frac{l\sigma}{\rho_f U_w} B_0^2$ (Magnetic field parameter),

$K = \frac{\mu l}{U_w \rho_f k}$ (porous media parameter),

where $v_w = \sqrt{\frac{2l}{\nu U_w}}\beta$ is the suction / injection parameter (v_w> 0 for suction and v_w < 0 for injection).

In the case of λ = 0, when the magnetic field, porous medium, viscous dissipation, heat generation and chemical reaction are not considered, we have the work of Nadeem and Lee [16]

Physical quantities of interest are Local skin frication c_f, Local Nusselt number Nu and Local Sherwood number Sh.

$$\left.\begin{aligned} \tau_w = \mu_0 \left[\frac{\partial u}{\partial y} + \frac{\Gamma}{\sqrt{2}}\left(\frac{\partial u}{\partial y}\right)^2\right]_{y=0}, \qquad c_f = \frac{\tau_w|_{y=0}}{\rho U_w^2}, \\ Nu = \frac{-x}{(T_w - T_\infty)}\frac{\partial T}{\partial y}\Big|_{y=0}, \qquad Sh = \frac{-x}{C_w - C_\infty}\frac{\partial C}{\partial y}\Big|_{y=0}, \end{aligned}\right\} \quad (32)$$

by introducing the transformations (27), we have

$$\sqrt{2Re}\,c_f = \left(f'' + \frac{\lambda}{2} f''^2\right)\Big|_{\eta=0}, \quad \frac{Nu}{\sqrt{Re}} = -\theta'(0), \quad \frac{Sh}{\sqrt{Re}} = -\phi'(0), \qquad (33)$$

where $Re = U_w l/\nu$ is the local Renolds number.

3. Numerical results and discussion

The coupled ordinary differential equations (24), (25) and (26) subjected to the boundary conditions (27) are solved numerically by using Runge-Kutta based shooting technique. Comprehensive numerical compulations have been carried out for various values of nondimensional governing parameters, namely Non-Newtonian parameter λ, magnetic field parameter *M*, Prandtl number *Pr*, Lewis number *Le*, Schmidt number S_c , Heat capacities ratio parameter N_c, Diffusivity ratio parameter N_{bt}, Brinkmen number B_r, Local Renolds number *Re*, Heat generation parameter Q, Chemical reaction parameter K_r and porous media parameter *K* on velocity, temperature and nanoparticle concentration profiles and then the results are presented in terms of graphs. The effect of the different parameters on the velocity profile *f'* when plotted against η is indicated graphically through figures [2-5]. The influence of the magnetic parameter on the velocity is shown in Fig.2. As magnetic parameter *M* increases, the velocity *f'*

decreases. This is because, an application of the magnetic field within the boundary layer produces a resistive-type force known as Lorentz force which opposes the flow, and decelerates the fluid motion. Fig. 3 shows the effect of porosity parameter *K* on velocity, it is observed that the velocity decreases as *K* increases. Physically, increasing the tightness of the porous medium which is represented by increase in *K* results in increasing the resistance against the flow and thus the fluid velocity decreased. Fig. 4 show the influence of the Non-Newtonian parameter λ on the velocity profile. The nanofluid velocity $f'(\eta)$ decrease with increasing λ which is not an unexpected result since it is well known that the viscoelastic fluid resists the motion of the fluid. The effect of velocity suction parameter v_w on the velocity is shown in Fig. 5. It is found that an icreases in suction parameter results a decrease in the velocity. Figures [6-16] illustrate the effects of *M, K,* λ*, Le,* N_c *, Pr,* B_r *, Re, Q,* $v_w$and N_{bt} on the temperature profiles of nanofluid θ. From Fig. 6 it is observed that increase in magnetic field parameter increases the temperature profiles. The reason behind this is increase in magnetic field reduces the boundary layer thickness and enhances the thermal conductivity of the fluid. The influences of the porosity parameter on the temperature profile θ is shown in Fig. 7. The temperature is increasing with increasing the dimensionless porosity parameter *K*. It can be observed from Fig. 8 that temperature increases with increase in λ. Fig. 9 demonstrate the effect of the Lewis number *Le* on temperature profile when other parameters are kept constant. Temperature profile decrease with the increase in *Le*. *Le* cannot be chosen equal to zero because it appears in the denominator of the Eq. (29). Physically *Le* cannot equal to zero since it is ratio of thermal diffusivity to Brownian diffusion. Fig. 10 describes the effect of heat capacities ratio *Nc* on the temperature profile. It is observed that temperature increase with the increase in *Nc*. If we look at the definition of *Nc*, it is the ratio of heat capacity of nano particles and nano fluid. Usually the specific heat C_p of nano particles is more than that of base fluid typically specific heat of solid is more than that of liquids. So addition of solid particles will increase the specific heat of base fluid, hence temperature profile increase. Fig. 11 shows that the temperature decrease with the increase in Prandtl number *Pr* . as we know *Pr* controls the relative thickness of momentum and themal boundary layer. Large *Pr* means smaller thermal boundary layer and larger momentum boundary layer. It can be observed from Fig. 12 that temperature profile increase with increase in viscous heating B_r , this is because B_r parameter enhance in thickening the thermal boundary layer. Fig. 13 shows that the temperature profile is increasing function of Reynold number *Re*. Fig. 14 shows that increasing heat generation parameter *Q* enhances the temperature profiles thereby increasing the thermal boundary layer thickness. The effect of suction parameter v_w on the temperature profile is shown in Fig. 15. It is found that an increase in suction parameter results a decrease in the temperature of the fluid. The influences of the diffusivity ratio *Nbt* parameter on the temperature profile θ is shown in Fig. 16. It is observed that the temperature and thermal boundary layer decrease with increase in *Nbt* . when Brownian diffusivity is very large as compared to thermophoretic diffusivity, temperature profile only shows very small variation. Figures [17-23] are drawn to examine the effects of important parameters on the nanoparticals volumetric fraction ϕ when plotted against η. Although some parameters are not directly involved in the nano particles volumetric fraction equation, buut there effects are appearing due to the coupling of Eqs.(25) and (26). Eq. (26) is second order equation in both θ and $\emptyset$. So value of *Nbt* will play the dominant rule when effects of parameters involved in θ and $\emptyset$. Figs. 17 ,18 and 19 shows that $\emptyset$ decrease with the increase in *Pr*, *Re* and *Q* . For different values of chemical reaction parameter K_r (>0), the concentration profiles are plotted in Fig. 20. An increase in chemical reaction parameter will suppress the concentration of the fluid. Higher values of K_r amount to a fall in the chemical molecular diffusivity, i.e., less diffusion. Therefore, they are obtained by species transfer. An increase in K_r will suppress species concentration. The concentration distribution decreases at all points of the flow field with the increase in the reaction parameter. Fig. 21 depicts the effect of Schmidt number on the concentration profile. As the Schmidt number *Sc* increases, the mass rate increases. Actually the Schmidt number is inversely proportional to the diffusion coefficient D_B. Hence, the concentration decreases with increasing S_c. Fig. 22 shows the influence of the diffusivity ratio *Nbt* parameter on the concentration profile. Since the Brownain and thermophoretic diffusion both cause the dispersion of particles across the boundary layer, thus the concentration profiles increase with increasing *Nbt* near the stretching sheet wall up-to a certain value of η but beyond this point, the opposite trend is observed. It means that concentration boundary layer thickness increases up-to a certain value of η but beyond this point it decreases.this is due to the revised nanoparticle concentration boundary condition. Fig. 23 displays the effects of the suction parameter v_w on the species concentration profiles. As the suction parameter increases the species concentration decreases. This is due to the usual fact that the suction stabilizes the boundary growth. Figures 24 and 25 the skin friction is plotted against magnetic field parameter M, it's observed from these figures that the skin friction is increase by increasing porosity parameter *K* and non-Newtonain parameter λ. Figure 26 illustrate the effect of magnetic field parameter *M* on the skin friction when it was plotted against porosity parameter *K*. It is found that the skin friction increases by increasing *M*. In figures [27-32] the Nusselt number distribution is plotted against *M*. It is observed from these figures that the Nusselt number decreases by increasing Pr, *K* and non-Newtonain parameter λ. whereas, it is increases by increasing Lewis number *Le*. Figures 31 and 32 are graphed to illustrate the effects of magnetic field parameter *M* and Brinkmen number B_r on the Nusselt number distribution when it was plotted against Permeability parameter K. It is found that the Nusselt number decreases by increasing M and

B_r. Figures [33-38] are graphed to illustrate the effects of *Pr, K, Le, M,* B_r and λ on the Sherwood number distribution. It is found that at fixed values of *M* the Sherwood number decreases with increasing *Le* and λ but it increases with increasing *Pr* and *K*. Also it's found from figures 36 and 37 that the Sherwood number at fixed values of *K* increases by increasing *M* and B_r .

Conclusion

In this work, the effect of magnetic field, viscous dissipation , heat generation and chemical reaction on boundary layer flow of nano Williamson fluid over a permeable exponentially stretching sheet through porous medium is investigated numerically. The governing equations are transformed into non-linear ordinary differential equations using similarity transformations and then solved numerically by Runge-Kutta with a shooting technique. A parametric study is performed to explore the effects of various governing parameters on skin fraction , heat and mass transfer characteristics. The very important results are:

- Increasing Prandtl number *Pr*, Local Renolds number *Re*, Heat generation parameter Q, Chemical reaction parameter K_r, Schmidt number S_c and suction parameter v_w lead o reduce the nanoparticle volume fraction near the boundary layer region but the effect is reverse for the diffusivity ratio *Nbt* .
- The fluid temperature increases for increasing magnetic field parameter *M,* porous media parameter *K,* non-Newtonain parameter λ, heat capacities ratio *Nc*, viscous heating B_r and Local Renolds number *Re* whereas the effect is opposite for Lewis number *Le* ,Prandtl number *Pr,* suction parameter v_w and diffusivity ratio *Nbt* .
- It is seen that the Nusselt number decreases while the Sherwood number increases as Prandtl number *Pr*, porosity parameter *K* , magnetic field parameter *M* and viscous heating B_r increase.
- A rise in the non-Newtonain parameter λ decreases both the rate of heat transfer and the rate of mass transfer at the stretching surface.
- Moreover, It is also observed that increase in Lewis number *Le* increases the Nusselt number whereas the opposite trend is noticed in the case of the Sherwood number .

Caption of figures:-

Figure (2)The velocity distribution is plotted against η for different values of M, with $\lambda = 0.1$, K = 3, Pr = 6.2, $N_c = 0.5$, Le = 4, $N_{bt} = 2$, $B_r = 0.3$, Re = 0.3, Q = 0.3, $S_c = 2$ and $K_r = 5$.

Figure (3)The velocity distribution is plotted against η for different values of K, with $\lambda = 0.1$, *M* = 0.5, Pr = 6.2, $N_c = 0.5$, Le = 4, $N_{bt} = 2$, $B_r = 0.3$, Re = 0.3, Q = 0.3, $S_c = 2$ and $K_r = 5$.

Figure (4)The velocity distribution is pl otted against η for different values of λ, with $M = 0.5$, K = 3, Pr = 6.2, $N_c = 0.5$, Le = 4, $N_{bt} = 2$, $B_r = 0.3$, Re = 0.3, Q = 0.3, $S_c = 2$ and $K_r = 5$.

Figure (5)The velocity distribution is pl otted against η for different values of v_w, with $\lambda = 0.1$, $M = 0.5$, K = 3, Pr = 6.2, $N_c = 0.5$, Le = 4, $N_{bt} = 2$, $B_r = 0.3$, Re = 0.3, Q = 0.3, $S_c = 2$ and $K_r = 5$.

Figure (6)The temperature distribution is plotted against η for different values of *M*, with $\lambda = 0.1$, K = 3, Pr = 6.2, $N_c = 0.5$, Le = 4, $N_{bt} = 2$, $B_r = 0.3$, Re = 0.3, Q = 0.3, $S_c = 2$ and $K_r = 5$.

Figure (7)The temperature distribution is plotted against η for different values of *K*, with $\lambda = 0.1$, *M* = 0.5, Pr = 6.2, $N_c = 0.5$, Le = 4, $N_{bt} = 2$, $B_r = 0.3$, Re = 0.3, Q = 0.3, $S_c = 2$ and $K_r = 5$.

Figure (8)The temperature distribution is plotted against η for different values of λ, with $M = 0.5$, *K = 3, Pr = 6.2,* $N_c = 0.5$, *Le = 4,* $N_{bt} = 2$, $B_r = 0.3$, *Re = 0.3, Q = 0.3,* $S_c = 2$ *and* $K_r = 5$.

Figure (9)The temperature distribution is plotted against η for different values of *Le*, with $M = 0.5$, *K = 3, Pr = 6.2,* $N_c = 0.5$, *λ= 0.1,* $N_{bt} = 2$, $B_r = 0.3$, *Re = 0.3, Q = 0.3,* $S_c = 2$ *and* $K_r = 5$.

Figure (10)The temperature distribution is plotted against η for different values of N_c, with $\lambda = 0.1$, *K = 3, Pr = 6.2,* $M = 0.5$, *Le = 4,* $N_{bt} = 2$, $B_r = 0.3$, *Re = 0.3, Q = 0.3,* $S_c = 2$ *and* $K_r = 5$.

Figure (11)The temperature distribution is plotted against η for different values of Pr, *with* $\lambda = 0.1$, *K = 3, M = 6.2,* $N_c = 0.5$, *Le = 4,* $N_{bt} = 2$, $B_r = 0.3$, *Re = 0.3, Q = 0.3,* $S_c = 2$ *and* $K_r = 5$.

Figure (12)The temperature distribution is plotted against η for different values of B_r, with $\lambda = 0.1$, *K = 3, Pr = 6.2,* $N_c = 0.5$, *Le = 4,* $N_{bt} = 2$, $M = 0.5$, *Re = 0.3, Q = 0.3,* $S_c = 2$ *and* $K_r = 5$.

Figure (13)The temperature distribution is plotted against η for different values of Re, with $\lambda = 0.1$, K = 3, Pr = 6.2, $N_c = 0.5$, Le = 4, $N_{bt} = 2$, $B_r = 0.3$, M = 0.5, Q = 0.3, $S_c = 2$ and $K_r = 5$.

Figure (14)The temperature distribution is plotted against η for different values of Q, with $\lambda = 0.1$, K = 3, Pr = 6.2, $N_c = 0.5$, Le = 4, $N_{bt} = 2$, $B_r = 0.3$, Re = 0.3, M = 0.5, $S_c = 2$ and $K_r = 5$.

Figure (15)The temperature distribution is plotted against η for different values of v_w , with $K_r = 5$, $\lambda = 0.1$, K = 3, Pr = 6.2, $N_c = 0.5$, Le = 4, $N_{bt} = 2$, $B_r = 0.3$, Re = 0.3, Q = 0.3, $S_c = 2$ and $M = 0.5$.

Figure (16)The temperature distribution is plotted against η for different values of N_{bt} , with $K_r = 5$, $\lambda = 0.1$, K = 3, Pr = 6.2, $N_c = 0.5$, Le = 4, $B_r = 0.3$, Re = 0.3, Q = 0.3, $S_c = 2$ and $M = 0.5$.

Figure (17) The nanoparticals concentration distribution is plotted against η for different values of Pr, with $\lambda = 0.1$, M = 0.5, Pr = 6.2, $N_c = 0.5$, Le = 4, $N_{bt} = 2$, $B_r = 0.3$, Re = 0.3, Q = 0.3, $S_c = 2$ and $K_r = 5$.

Figure (18) The nanoparticals concentration distribution is plotted against η for different values of Re, with $\lambda = 0.1$, K = 3, Pr = 6.2, $N_c = 0.5$, Le = 4, $N_{bt} = 2$, $B_r = 0.3$, Re = 0.3, Q = 0.3, $S_c = 2$ and $K_r = 5$.

Figure (19) The nanoparticals concentration distribution is plotted against η for different values of Q, with $\lambda = 0.1$, K = 3, Pr = 6.2, $N_c = 0.5$, Le = 4, $N_{bt} = 2$, $B_r = 0.3$, Re = 0.3, M = 0.5, $S_c = 2$ and $K_r = 5$.

Figure (20) The nanoparticals concentration distribution is plotted against η for different values of K_r, with $\lambda = 0.1$, K = 3, Pr = 6.2, $N_c = 0.5$, Le = 4, $N_{bt} = 2$, $B_r = 0.3$, Re = 0.3, Q = 0.3, $S_c = 2$ and $M = 0.5$.

Figure (21) The nanoparticals concentration distribution is plotted against η for different values of S_c, with $\lambda = 0.1$, K = 3, Pr = 6.2, $N_c = 0.5$, Le = 4, $N_{bt} = 2$, $B_r = 0.3$, Re = 0.3, Q = 0.3, $M = 0.5$ and $K_r = 5$.

Figure (22) The nanoparticals concentration distribution is plotted against η for different values of N_{bt}, with $\lambda = 0.1$, K = 3, Pr = 6.2, $N_c = 0.5$, Le = 4, $M = 0.5$, $B_r = 0.3$, Re = 0.3, Q = 0.3, $S_c = 2$ and $K_r = 5$.

Figure (23) The nanoparticals concentration distribution is plotted against η for different values of v_w, with $\lambda = 0.1$, K = 3, Pr = 6.2, $N_c = 0.5$, Le = 4, $M = 0.5$, $B_r = 0.3$, Re = 0.3, Q = 0.3, $S_c = 2$, M = 0.5 and $K_r = 5$.

Figure (24) The skin friction distribution is plotted against M for different values of *K*, with $\lambda = 0.1$, K = 3, Pr = 6.2, $N_c = 0.5$, Le = 4, $N_{bt} = 2$, $B_r = 0.3$, Re = 0.3, Q = 0.3, $S_c = 2$ and $K_r = 5$.

Figure (25) The skin friction distribution is plotted against M for different values of λ, with $\lambda = 0.1$, K = 3, Pr = 6.2, $N_c = 0.5$, Le = 4, $N_{bt} = 2$, $B_r = 0.3$, Re = 0.3, Q = 0.3, $S_c = 2$ and $K_r = 5$.

Figure (26) The skin friction distribution is plotted against *K* for different values of M, with $\lambda = 0.1$, K = 3, Pr = 6.2, $N_c = 0.5$, Le = 4, $N_{bt} = 2$, $B_r = 0.3$, Re = 0.3, Q = 0.3, $S_c = 2$ and $K_r = 5$.

Figure (27) The Nusselt number distribution is plotted against M for different values of P_r, with $\lambda = 0.1$, K = 3, Pr = 6.2, $N_c = 0.5$, Le = 4, $N_{bt} = 2$, $B_r = 0.3$, Re = 0.3, Q = 0.3, $S_c = 2$ and $K_r = 5$.

Figure (28) The Nusselt number distribution is plotted against M for different values of *K*, with N_c $\lambda = 0.1$, K = 3, Pr = 6.2, $N_c = 0.5$, Le = 4, $N_{bt} = 2$, $B_r = 0.3$, Re = 0.3, Q = 0.3, $S_c = 2$ and $K_r = 5$.

Figure (29) The Nusselt number distribution is plotted against M for different values of Le, with $\lambda = 0.1$, K = 3, Pr = 6.2, $N_c = 0.5$, Le = 4, $N_{bt} = 2$, $B_r = 0.3$, Re = 0.3, Q = 0.3, $S_c = 2$ and $K_r = 5$.

Figure (30) The Nusselt number distribution is plotted against M for different values of λ, with $M = 0.5$, K = 3, Pr = 6.2, $N_c = 0.5$, Le = 4, $N_{bt} = 2$, $B_r = 0.3$, Re = 0.3, Q = 0.3, $S_c = 2$ and $K_r = 5$.

Figure (31) The Nusselt number distribution is plotted against K for different values of M, with $\lambda = 0.1$, K = 3, Pr = 6.2, $N_c = 0.5$, Le = 4, $N_{bt} = 2$, $B_r = 0.3$, Re = 0.3, Q = 0.3, $S_c = 2$ and $K_r = 5$.

Figure (32) The Nusselt number distribution is plotted against K for different values of B_r, with $\lambda = 0.1$, M = 0.5, Pr = 6.2, $N_c = 0.5$, Le = 4, $N_{bt} = 2$, $B_r = 0.3$, Re = 0.3, Q = 0.3, $S_c = 2$ and $K_r = 5$.

Figure (33) The Sherwood number distribution is plotted against M for different values P_r , with $\lambda = 0.1$, K = 3, Pr = 6.2, $N_c = 0.5$, Le = 4, $N_{bt} = 2$, $B_r = 0.3$, Re = 0.3, Q = 0.3, $S_c = 2$ and $K_r = 5$.

Figure (34) The Sherwood number distribution is plotted against M for different values K , with $\lambda = 0.1$, K = 3, Pr = 6.2, $N_c = 0.5$, Le = 4, $N_{bt} = 2$, $B_r = 0.3$, Re = 0.3, Q = 0.3, $S_c = 2$ and $K_r = 5$.

Figure (35) The Sherwood number distribution is plotted against M for different values Le, with $\lambda = 0.1$, K = 3, Pr = 6.2, $N_c = 0.5$, Le = 4, $N_{bt} = 2$, $B_r = 0.3$, Re = 0.3, Q = 0.3, $S_c = 2$ and $K_r = 5$.

Figure (36) The Sherwood number distribution is plotted against K for different values M, with $\lambda = 0.1$, K = 3, Pr = 6.2, $N_c = 0.5$, Le = 4, $N_{bt} = 2$, $B_r = 0.3$, Re = 0.3, Q = 0.3, $S_c = 2$ and $K_r = 5$.

Figure (37) The Sherwood number distribution is plotted against K for different values B_r, with N_c = 0.5, K = 1, $S_c = 6$, Le $= 4$, P_r = 10, Re = 0.1, $K_r = 10$ and Q $= 0.1$, N_{bt}=0.5.

Figure (38) The Sherwood number distribution is plotted against M for different values of λ, with $M = 0.5$, K = 3, Pr = 6.2, $N_c = 0.5$, Le = 4, $N_{bt} = 2$, $B_r = 0.3$, Re = 0.3, Q = 0.3, $S_c = 2$ and $K_r = 5$.

Figure 2

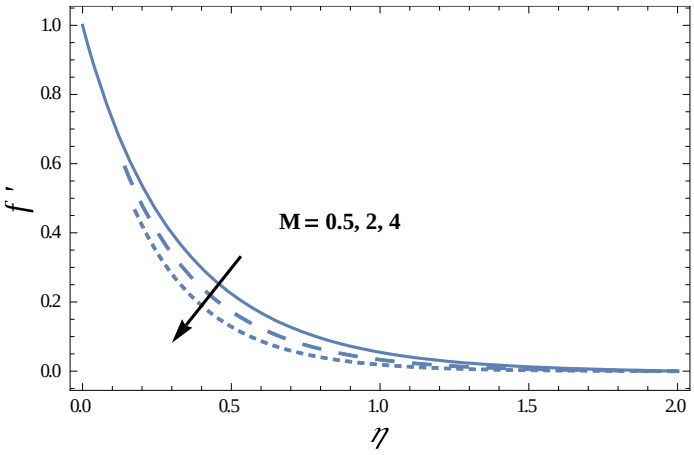

Figure 3

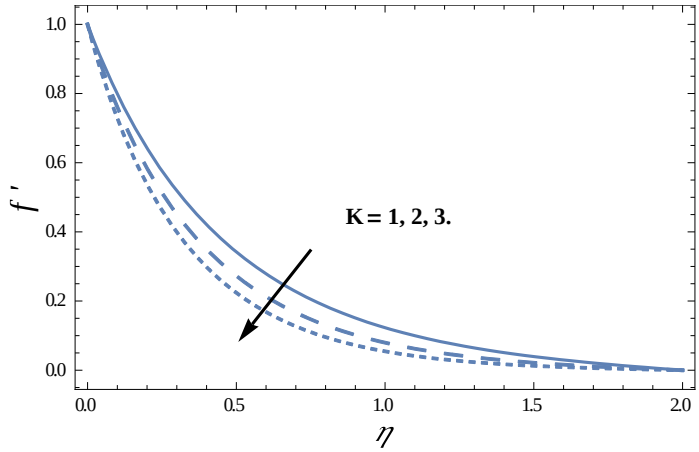

Figure 4

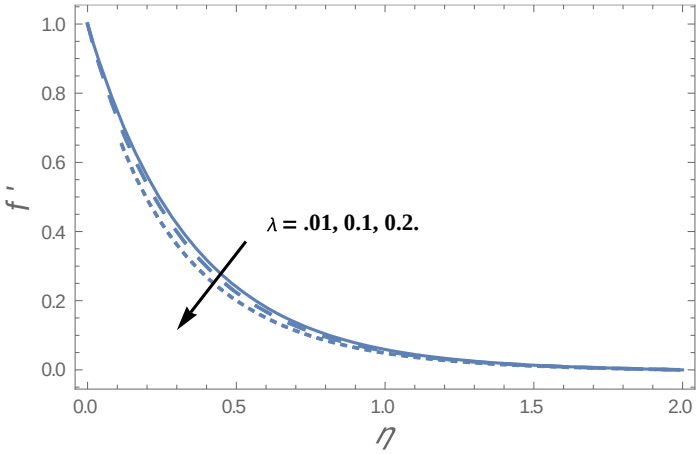

Figure 5

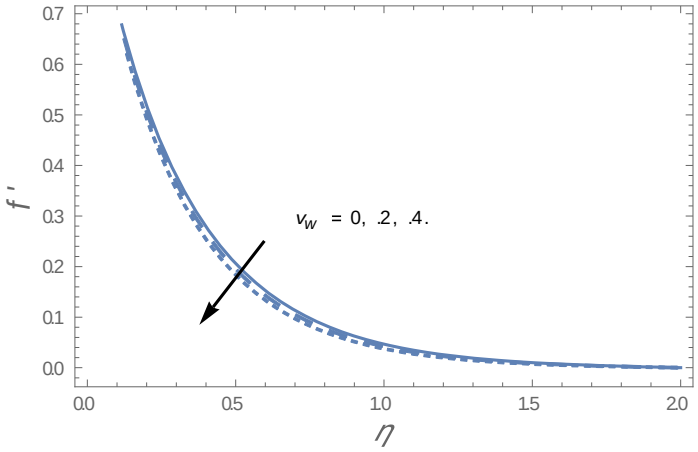

Figure 6

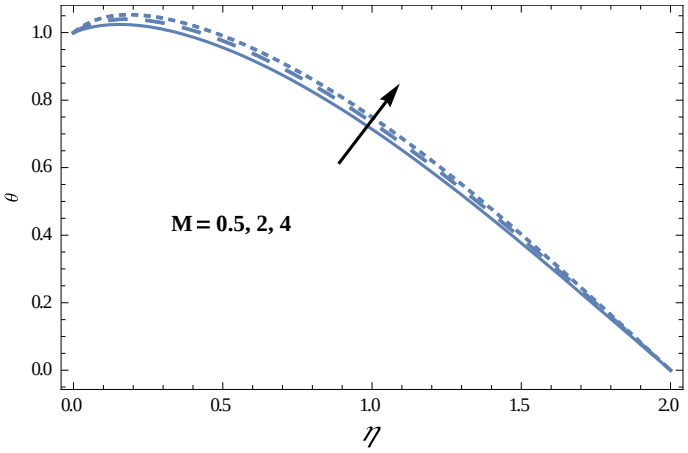

Figure 7

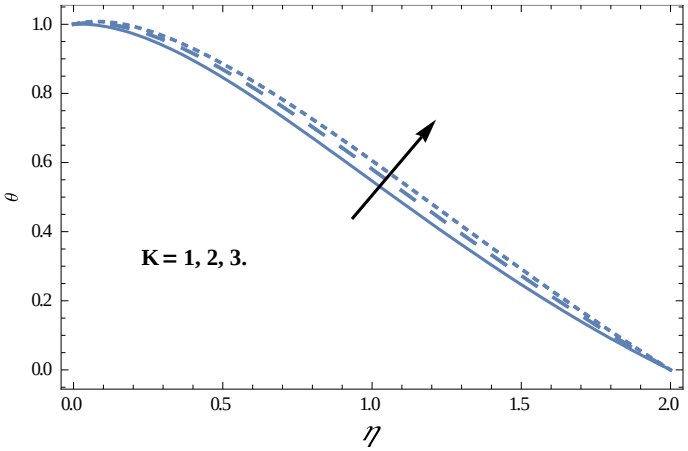

Figure 8

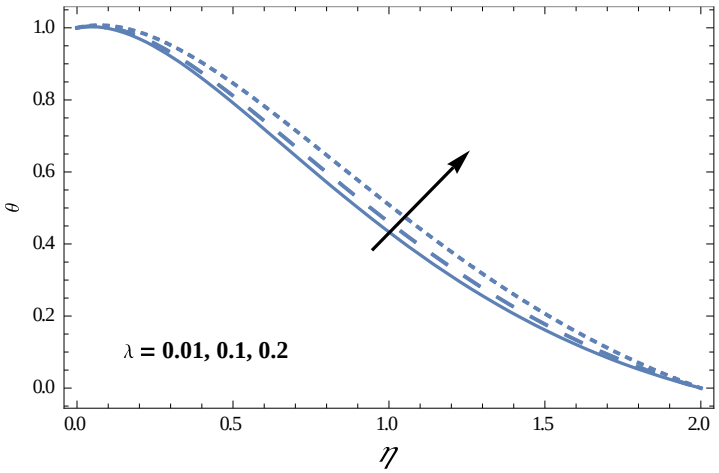

Figure 9

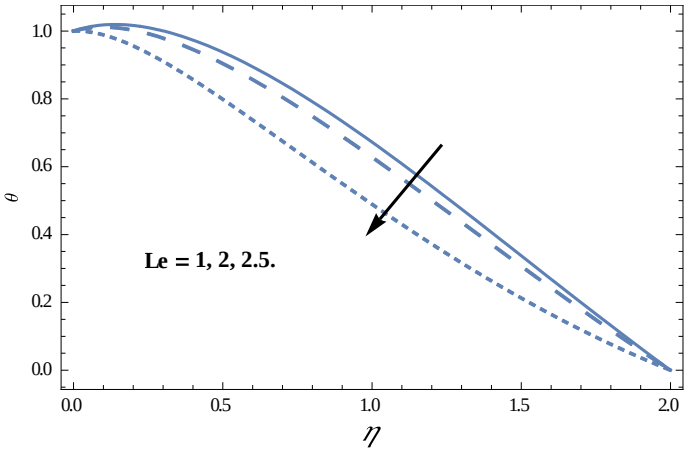

Figure 10

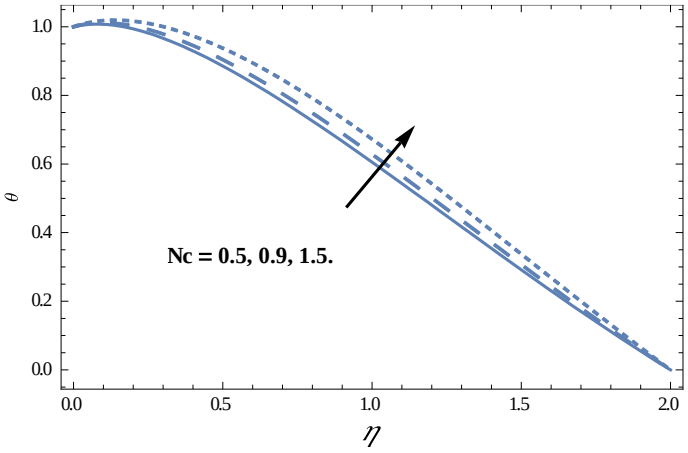

Figure 11

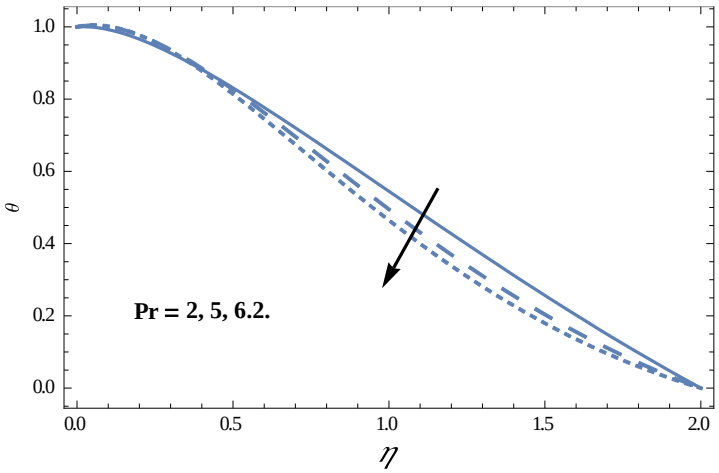

Figure 12

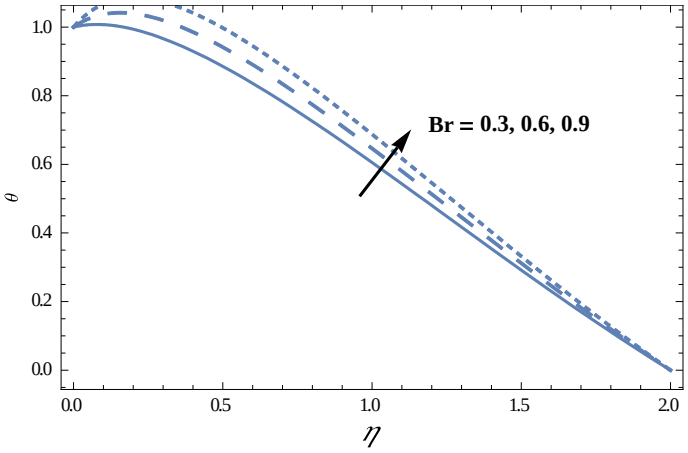

Figure 13

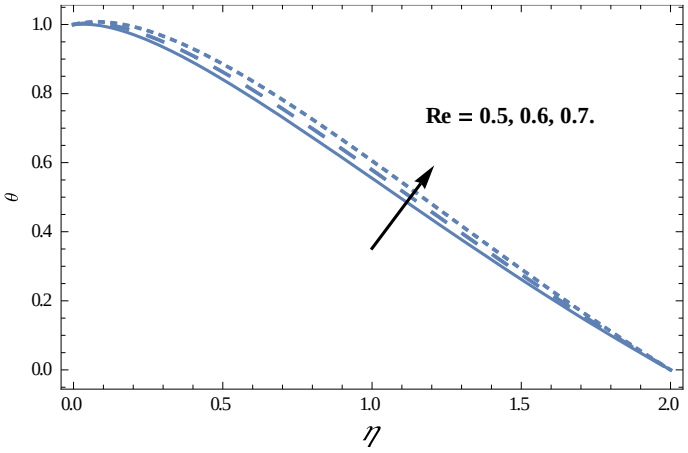

Figure 14

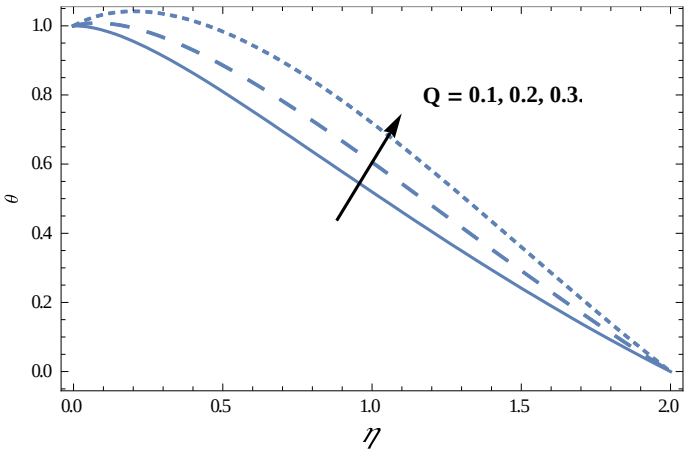

Figure 15

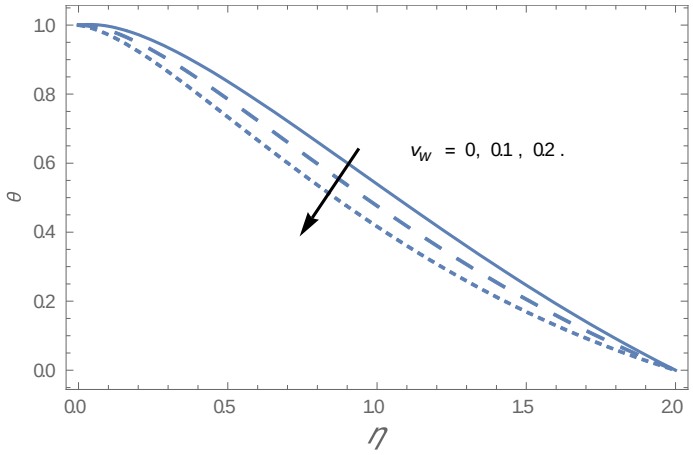

Figure 16

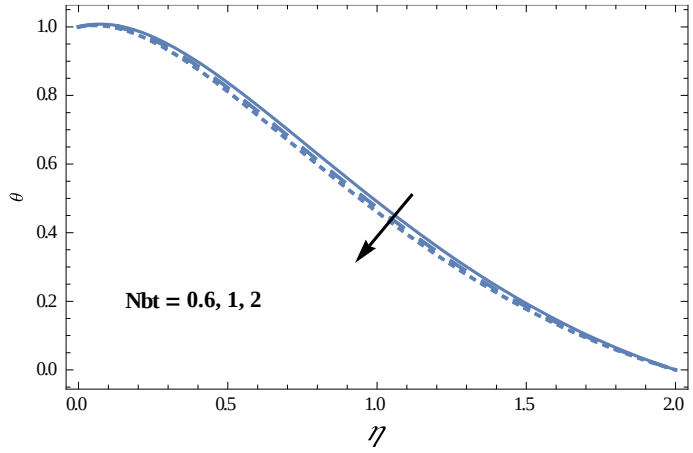

Figure 17

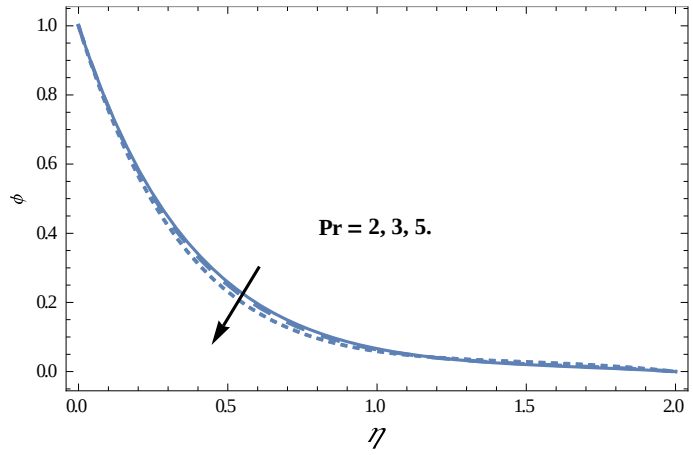

Figure 18

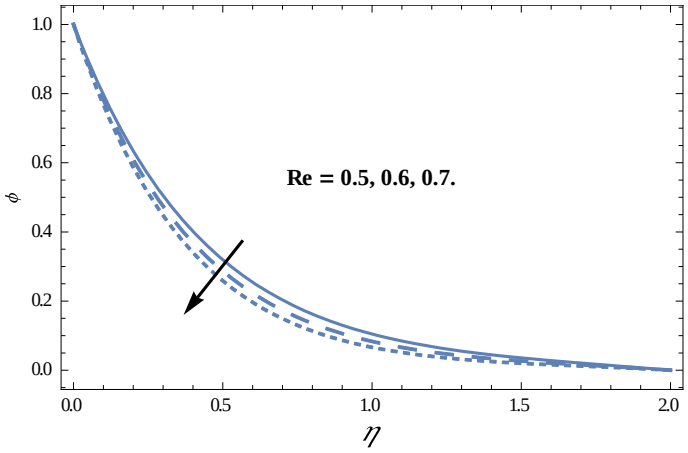

Figure 19

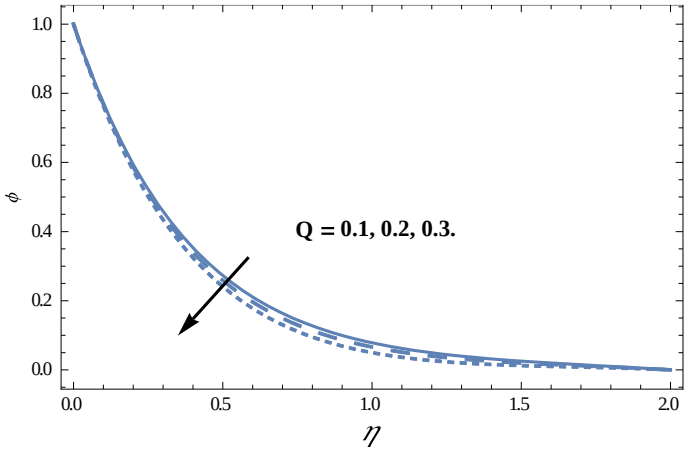

Figure 20

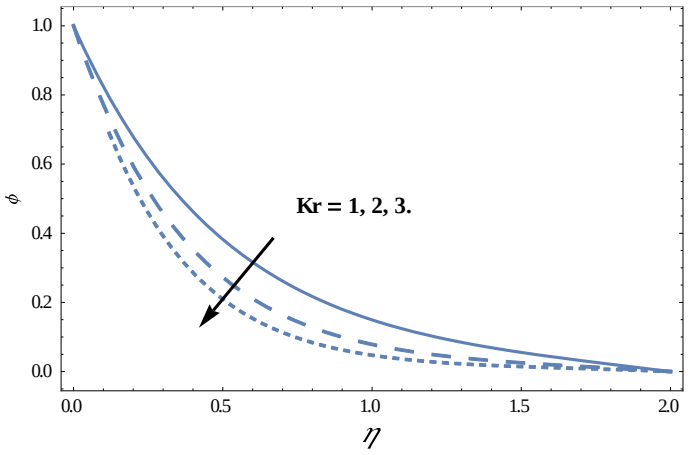

Figure 21

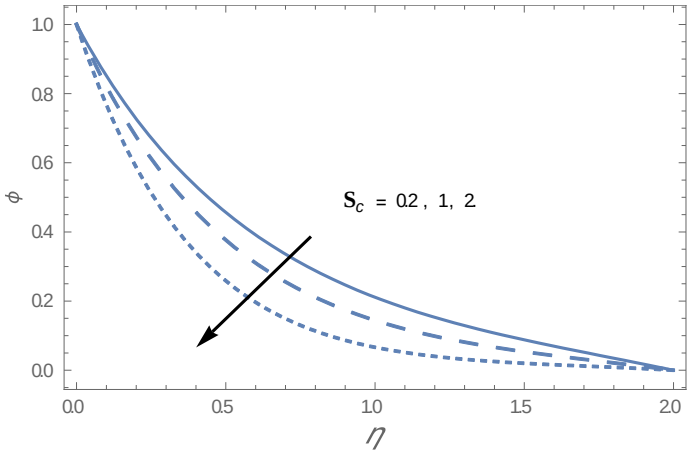

Figure 22

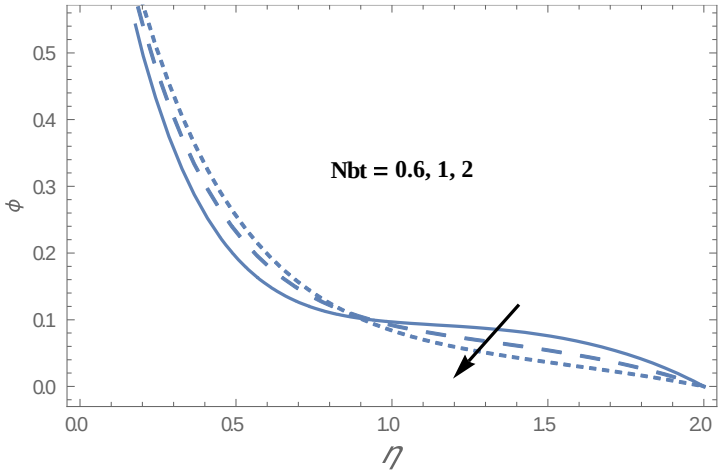

Figure 23

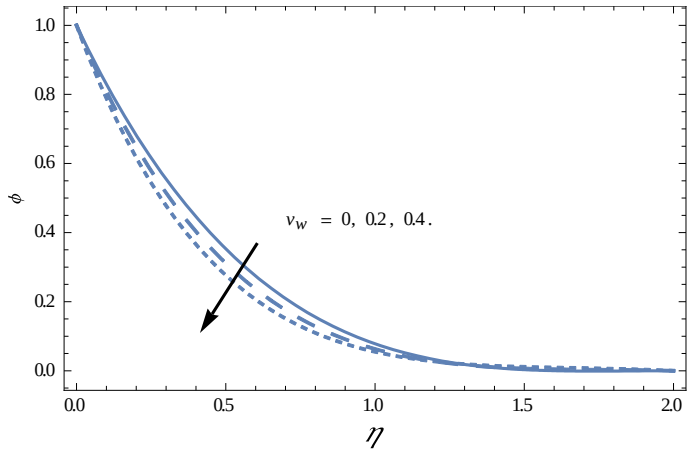

Figure 24

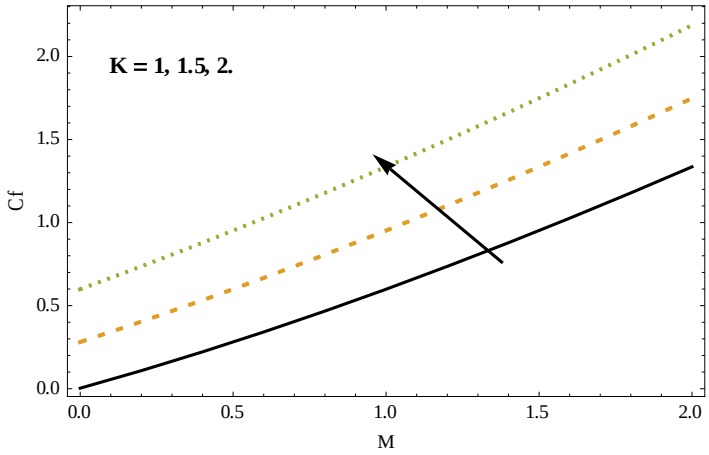

Figure 25

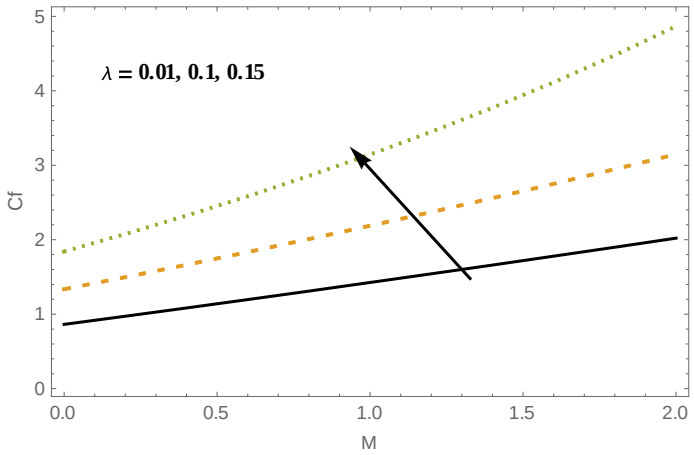

Figure 26

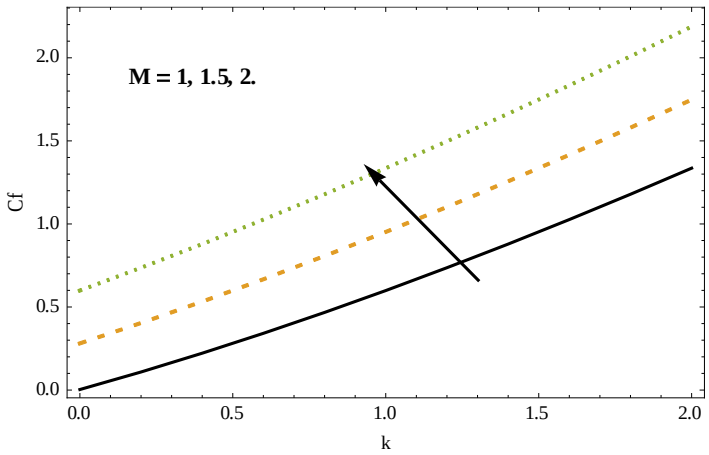

Figure 27

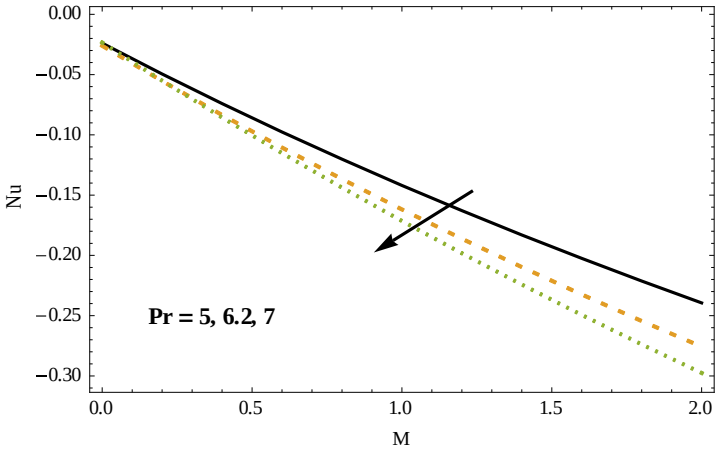

Figure 28

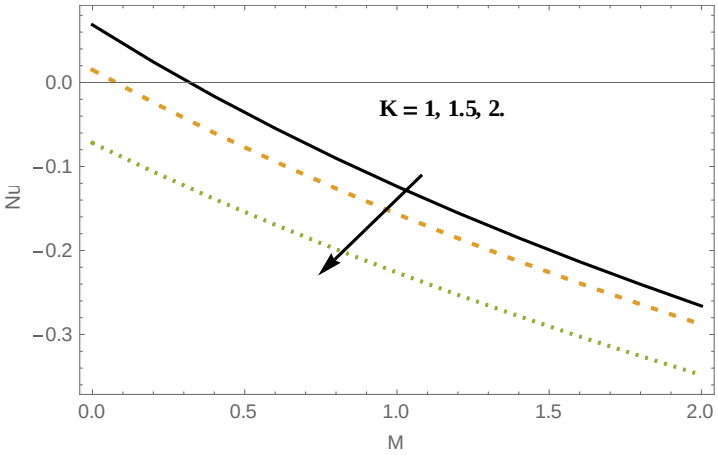

Figure 29

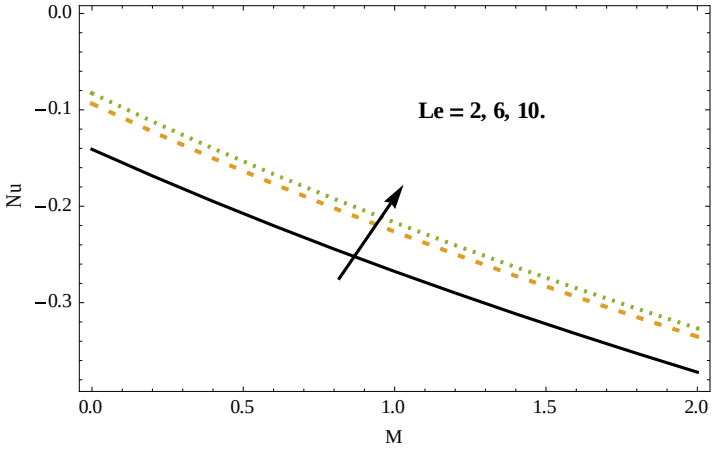

Figure 30

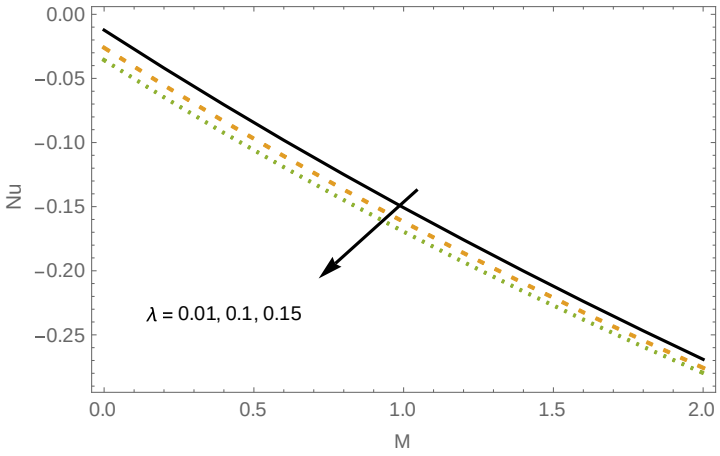

Figure 31

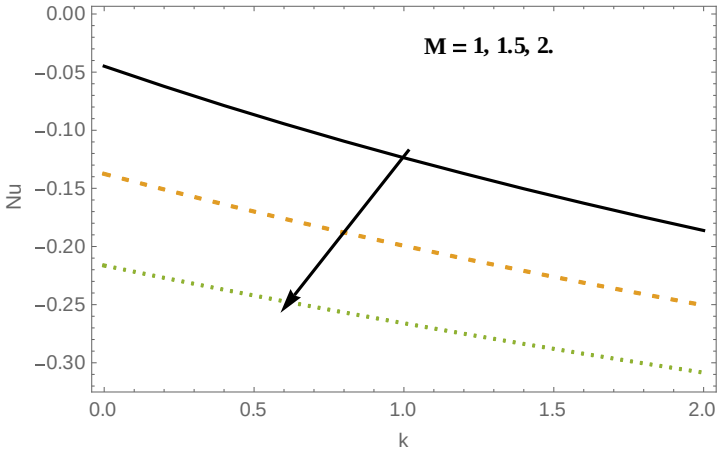

Figure 32

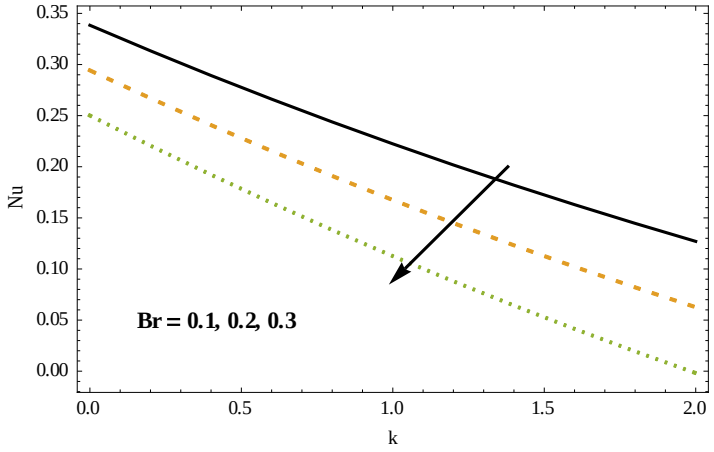

Figure 33

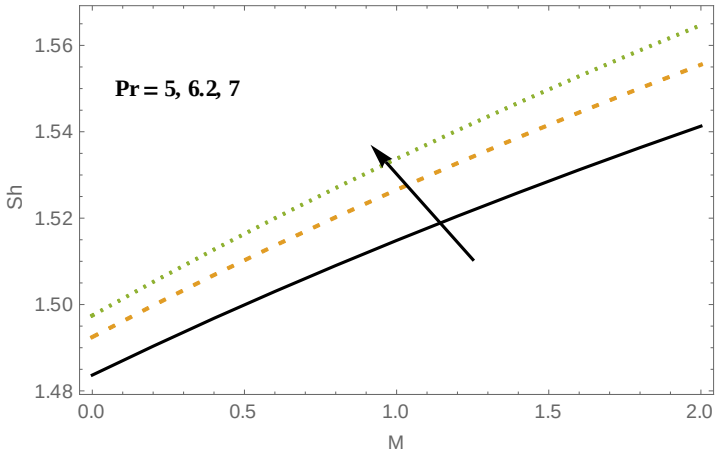

Figure 34

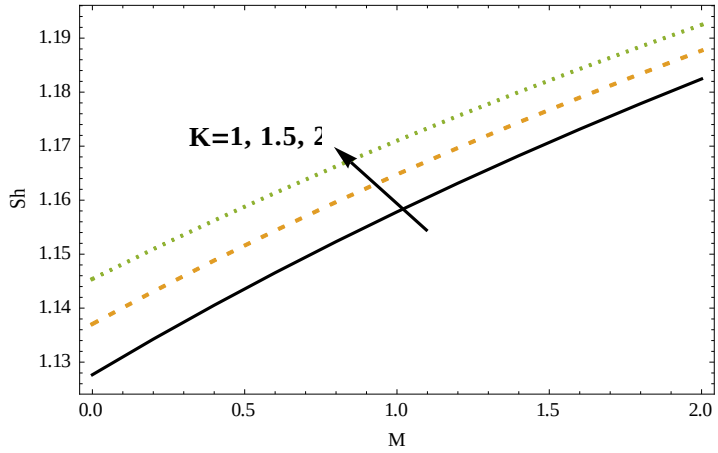

Figure 35

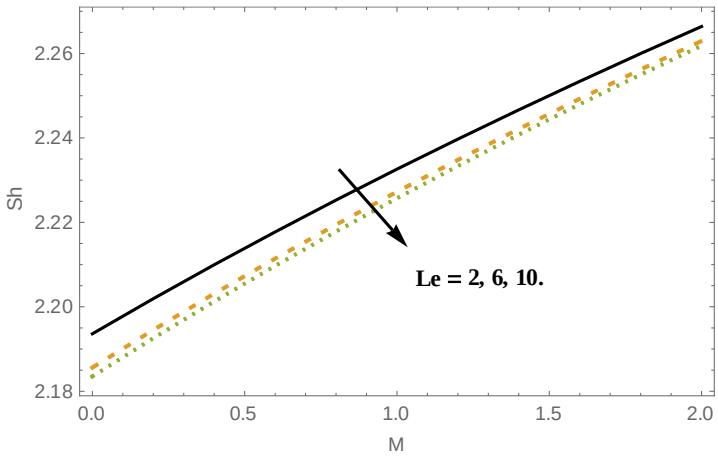

Figure 36

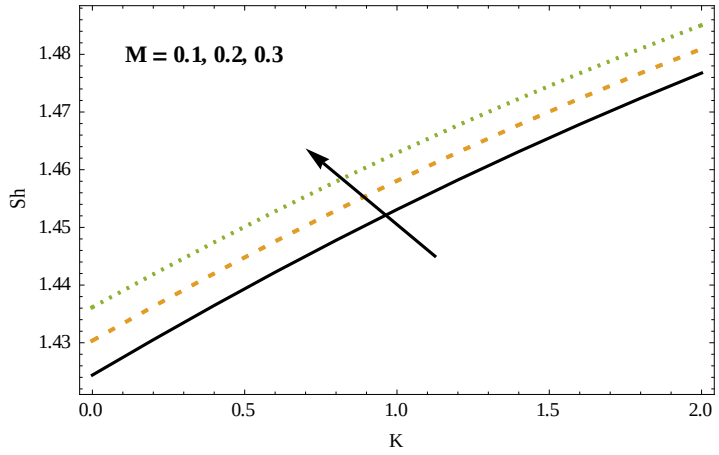

Figure 37

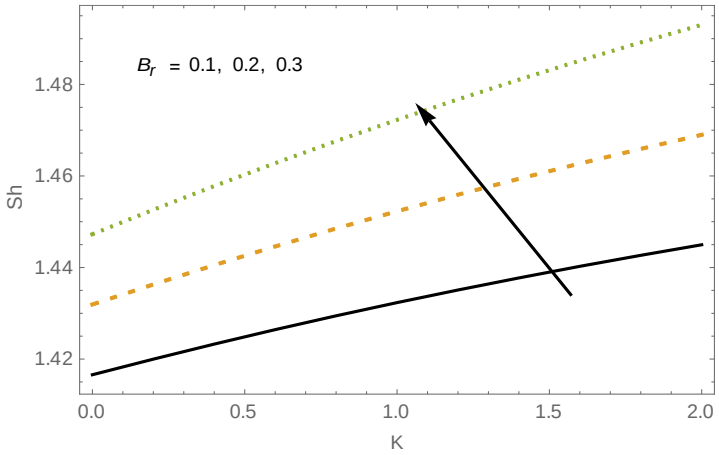

Figure 38

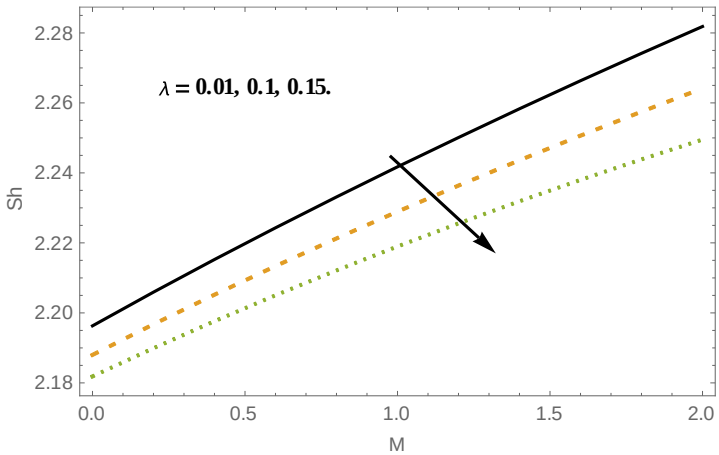

References

[1] Buongiorno J."Convective transport in nanofluids" *ASME J. Heat, Transfer,* vol. 128, pp. 240-250, 2006.
[2] Khan W. A. and Pop I. " Boundary-layer flow of a nanofluid past a stretching sheet" *Int. J. Heat Mass Transfer,* vol. 53, pp. 2477-2483, 2010.
[3] Kuznetsov A. V. and Nield D. A. "Natural convective boundary layer flow of a nanofluid past a vertical plate" *Int. J. Therm Sci.,* vol. 49, pp. 243-7, 2010.
[4] Gorla R.S.R. and Chamkha A."Natural convective boundary layer flow over a horizontal plat embedded in a porous medium saturated with a nanofluid" *J. Modern Phys,* vol. 2, pp. 62-71, 2011.
[5] Swati M."Slip effects on MHD boundary layer flow over an exponentially stretching sheet with suction/blowing and thermal radiation" *Ain Shams Eng, J.* vol. 4, pp. 485-491, 2013.
[6] Haroun Nageeb AH, Mondal S. and Sibanda Precious"unsteady natural convective boundary-layer flow of MHD nanofluid over a stretching surfaces with chemical reaction using the spectral relaxation method a revised model" *Procedia Eng,* vol. 127, pp. 18-24, 2015.
[7] Kiran Kumar RVMSS, Durga Prasad P and Varma SVK"Analytical study of heat and mass transfer enhancement in free convection flow with chemical reaction and constant heat source in nanofluids" *Pocedia Eng* vol. 127, pp. 978-85, 2015.
[8] Kiran Kumar RVMSS, Durga Prasad P and Varma SVK "Thermo-diffusion and chemical reaction effects on free convective heat and mass transfer flow of conducting nanofluid through porous medium in a rotating frame" *Global J Pure Appl Math,* vol. 12, pp. 342-51, 2016
[9] Williamson, R. V.,"The flow of pseudoplastic materials" *Industrial & Engineering Chemistry Research,* vol. 21, pp. 1108, 1929.
[10] Lyubimov, D. V. and A. V. Perminov,"Motion of a thin oblique layer of a pseudoplastic fluid" *Journal of Engineering Physics and Thermophysics,* vol. 75, pp.920, 2002.
[11] Dapra and G. Scarpi,"Pertubation solution for pulsatile flow of a non-NewtonianWilliamoson fluid in a rock frature" *International Journal of Rock Mechanics and Mining Sciences,* vol. 44, pp. 271, 2007.
[12] Nadeem S. and Akram,S."Peristaltic flow of a Williamson fluid in an asymmetric channel"*Communications in Nonlinear Science and Numerical Simulation,* vol. 15, pp. 475, 2010.
[13] Vasudev C. R. U. Rao, M. V. S. Reddy and G. P. Rao,"Peristaltic pumping of Williamson fluid through a porous medium in a horizontal channel with heat transfer" *American Journal of Scientific and Industrial Research,* vol. 1, pp. 656, 2010.
[14] Cramer S. D. and J. M. Marchello,"Numerical evaluation of models describing non-Newtonian behavior" *American Institute of Chemical Engineers Journal,* vol. 14, pp. 980, 1968.
[15] Schliching H. *Boundary Layer Theory,* McGraw-Hill, New York, 1964.
[16] Nadeem S, Lee C. *Nanoscale Res Lett* , 7:94,2012.